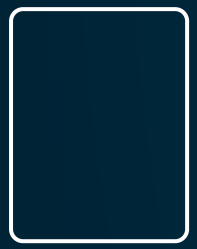

Springer

Sensing and Imaging

Publishing model

Hybrid

Submit your manuscript

Explore open access funding | Select institution

Journal menu

About this journal

Aims and scope

Editorial board

Editorial policies

Ethics and disclosures

Rights and permissions

Contact the journal

Articles

Articles

Collections

Volumes and issues

Sign up for alerts

For authors

Pre-submission checklist

Submission guidelines

How to publish with us

Fees and funding

Calls for papers

Language editing

Submit your manuscript

Journal updates

Overview

Sensing and Imaging is a peer-reviewed journal focusing on theoretical and experimental advancements in sensing and imaging technologies in engineering and science.The journal has a broad and multidisciplinary scope, including all varieties of sensor technology (physical, chemical, and biological) and relevant image/video processing techniques, and all areas of applications.

- Covers subsurface and surface sensing, along with systems, networks, and applications in engineering, science, and medicine.
- Describes the detection, identification, and classification of objects, structures, and matter under and at surfaces.
- Overseen by an international Editorial Board representing the full scope of the journal.
- Offers open access publishing at no cost to corresponding authors from participating institutions through Springer Nature Transformative agreements.

Editors-in-Chief

Journal metrics

Journal Impact Factor
2.0 (2024)

5-year Journal Impact Factor
1.9 (2024)

Submission to first decision (median)
12 days

Downloads
53.6k (2024)

Nathan Ida
Ming Jiang

View all editors →

Calls for papers

Collection

Special Issue on the Advances in Remote Sensing for Inland Water Monitoring

Inland water bodies such as lakes, reservoirs, rivers, and wetlands play critical roles in global hydrological processes, biodiversity...

Open for submissions

Submission deadline
31 March 2026

Collection

ICSI 2024: Recent developments in Sensing and Imaging (invited papers only)

The Sensing and Imaging journal encourages researchers from either academia or industry in the fields of sensing and imaging as well as related...

Open for submissions

Submission deadline
28 February 2026

View all calls for papers →

Sign up for alerts

Get notified when new articles are published.

Latest articles

Optimization of Refractive Index-Driven Optical Fiber Sensor Performance Based on Double Perovskite Halides for Cancer Detection

Research | 23 January 2026 | Article: 20

Design and Simulation of a DBR Structure based Tamm Plasmon Refractive Index Sensor for Cancer Cell Detection

Research | 23 January 2026 | Article: 19

Graphene-Enhanced V-Shaped Metasurface Resonators for High-Sensitivity Refractive Index Sensing: Electromagnetic Modeling and Machine-Learning Validation

Research | 21 January 2026 | Article: 18

Graphene–Copper Hybrid Terahertz Biosensor with KNN Sensitivity Optimization for Early Skin Cancer (Melanoma) Detection

Research | 17 January 2026 | Article: 17

A Multi-scale Convolutional Neural Network for Precise Digital Terrain Model Extraction from Digital Surface Models

Research | 12 January 2026 | Article: 16

View all articles →

This journal has 29 open access articles →

Journal updates

Congratulations Editors-in-Chief of Sensing and Imaging

Congratulations to Ming Jiang and Nathan Ida! Sensing and Imaging is a top rated Springer Nature journal.

View all updates →

Journal information

Electronic ISSN

1557-2072

Abstracted and indexed in

AGRICOLA
Astrophysics Data System (ADS)
BFI List
Baidu
CLOCKSS
CNKI
CNPIEC
Chinese Academy of Medical Science (CAMS)
Dimensions
EBSCO
EI Compendex
EMBiology
Emerging Sources Citation Index
Google Scholar
INSPEC

Japanese Science and Technology Agency (JST)

Naver

Norwegian Register for Scientific Journals and Series

OCLC WorldCat Discovery Service

Portico

ProQuest

SCImago

SCOPUS

TD Net Discovery Service

Wanfang

eLibrary.ru

Search

Search by keyword or author

Navigation

Find a journal

Publish with us

Track your research

Sensing and Imaging

Publishing model: **Hybrid**

Volume 27, Issue 1

December 2026

20 articles in this issue

Optimization of Refractive Index-Driven Optical Fiber Sensor Performance Based Perovskite Halides for Cancer Detection

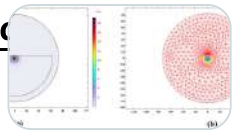

Research | 23 January 2026 | Article: 20

Design and Simulation of a DBR Structure based Tamm Plasmon Refractive Index Cancer Cell Detection

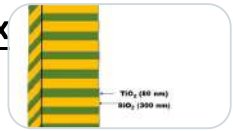

Research | 23 January 2026 | Article: 19

Graphene-Enhanced V-Shaped Metasurface Resonators for High-Sensitivity Ref Index Sensing: Electromagnetic Modeling and Machine-Learning Validation

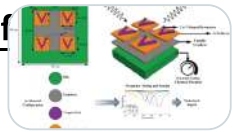

Research | 21 January 2026 | Article: 18

Graphene–Copper Hybrid Terahertz Biosensor with KNN Sensitivity Optimizatio Skin Cancer (Melanoma) Detection

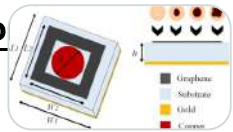

Research | 17 January 2026 | Article: 17

A Multi-scale Convolutional Neural Network for Precise Digital Terrain Model Ext Digital Surface Models

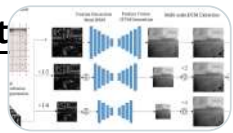

Research | 12 January 2026 | Article: 16

IoMT-Based Compressive Sensing with Threshold Filtering for Healthcare Monit POCT Device

Research | 10 January 2026 | Article: 15

Dielectric Modulation-Based High-Sensitivity Biomolecular Detection Using Ge/ Heterostructure ES Fin-TFET Biosensors: A Detailed Performance Study

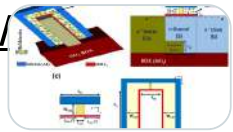

Research | 08 January 2026 | Article: 14

High Performance Terahertz Sensor Structure Based on Coupled MIM Waveguide Resonator Structure

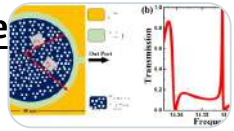

Research | 08 January 2026 | Article: 13

Blind-Spot Free Measurement Matrix for Compressed Sensing in Single-Path Ind of-Flight

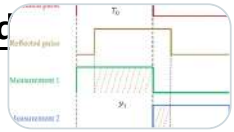

Research | 06 January 2026 | Article: 12

Efficient SPR-Based Cancer Cell Detection Using MgH_2 and CdSe Layers with Angu Interrogation Approach

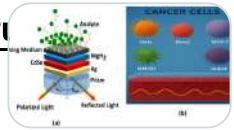

Research | 06 January 2026 | Article: 11

Performance Enhancement of an Optical SPR Sensor for the Detection of Cancero Cells

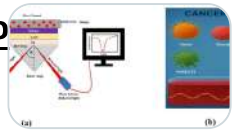

Research | 03 January 2026 | Article: 10

NO_2 Gas Sensing of Polypyrrole (PPy) Thin Film with Consequences of Relative Hu

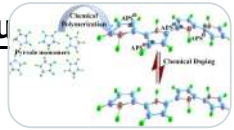

Research | 24 December 2025 | Article: 9

A Novel Mercury and Gallium Sulfide Assisted Surface Plasmon Resonance Sensor Enhanced Refractive Index Sensitivity

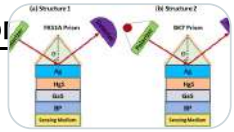

Research | 22 December 2025 | Article: 8

A Single-Port Microwave Sensor Based on Interdigital Capacitor and Electromagn Coupled Structure for Permittivity Detection of Vegetables Materials

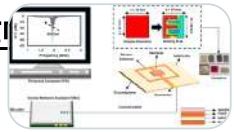

Research | 22 December 2025 | Article: 7

An Encoder-Decoder Architecture for Polyp Segmentation from Gastrointestinal Images

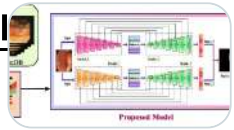

Research | 22 December 2025 | Article: 6

Image Reconstruction Method Based on Split Bregman Iteration for Solving EMT Regularizers Inverse Problem

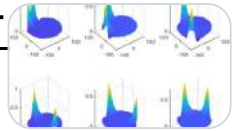

Research | 22 December 2025 | Article: 5

Fast GAN Based Iterative Motion Estimation for Tomographic Imaging Modalities

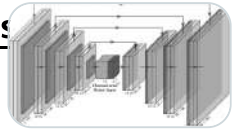

Research | Open access | 22 December 2025 | Article: 4

Enhancing Cognitive Functions in Aged Rats Through Red Light Stimulation: A Fo Hippocampal-Thalamic Interaction

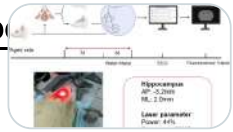

Research | 22 December 2025 | Article: 3

Part of 1 collection:

ICSI 2024: Recent developments in Sensing and Imaging (invited papers only)

Multilayer Implantable Antenna for Detecting Heart Muscle Damage in the MICS Band: A Preliminary Ex-Vivo Study

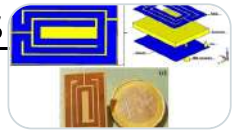

Research | 20 December 2025 | Article: 2

Correction: Automatic Multi-scale Dilated MobilenetV2 with Attention-Based Lung Nodule Detection Framework Using Adaptive 3D Trans-MobileUnet + + Segmentation

Correction | 16 December 2025 | Article: 1

Editorial board

Editors-in-Chief

Nathan Ida

University of Akron, Akron, United States

Ming Jiang
Peking University, Beijing, China

Founding Editor

Cam Nguyen
Dept. of Electrical Engineering, Texas A&M University, College Station, United States

Advisory Board

Gabor T. Herman
The Graduate Center, City University of New York, New York, United States

Peter Maaß
University of Bremen, Bremen, Germany

Eric Todd Quinto
Tufts University, Medford, United States

Editorial Board

Timothy Bechtel
Franklin & Marshall College, Lancaster, United States

Ping Chen
North University of China, Taiyuan, China

Peking University Third Hospital, Beijing, China; Shenzhen University Health Science Center, Shenzhen, China

Tingting Jiang
Peking University, Beijing, China

Tobias Kluth
University of Bremen, Bremen, Germany

Tuami Lasri
Institut d'Électronique et des Technologies du numéRique, Rennes, France

Yann Le Bihan
Université Paris-Saclay, Gif-sur-Yvette, France

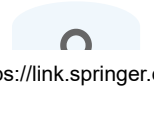

University of Science and Technology of China, Hefei, China

Lucas Travassos
Universidade Federal de Santa Catarina, Florianópolis, Brazil

Benoît Vozel
Université de Rennes, Rennes, France

Qingguo Xie
University of Science and Technology of China, Hefei, China

Hao-Min Zhou
Georgia Institute of Technology, Atlanta, United States

Sensing and Imaging (2026) 27:7
https://doi.org/10.1007/s11220-025-00708-0

RESEARCH

A Single-Port Microwave Sensor Based on Interdigital Capacitor and Electromagnetic Coupled Structure for Permittivity Detection of Vegetables Materials

Fitri Kurnia Sari[1] · Syah Alam[1] · Indra Surjati[1] · R. Deiny Mardian[1] · Lydia Sari[1] · Muhammad Nugrah Kusumah[1] · Teguh Firmansyah[2] · Dwi Astuti Cahyasiwi[3] · Zahriladha Zakaria[4] · Noor Azwan Shairi[4]

Received: 11 September 2025 / Revised: 25 November 2025 / Accepted: 14 December 2025

Abstract

This research proposed a single port microwave sensor designed for permittivity detection of both solid and vegetable samples, utilizing an Electric Field Coupled (ELC) resonator combined with an Interdigital Capacitor (IDC) structure. The sensor operates at a centre frequency of 1.9 GHz and adopts a single-port configuration with a reflection coefficient (S_{11}) maintained below −10 dB. Permittivity measurement is achieved using perturbation theory, where a shift in the resonant frequency occurs when a material is introduced into the sensing region. This sensing region is defined by the location of maximum electric field concentration within the resonator. A polynomial fitting equation, derived from measurements on known dielectric materials with permittivity values ranging from 1 to 9.8, is used to estimate the permittivity of vegetable samples. The proposed sensor demonstrates high performance, with a measured accuracy of 98.94%, normalized sensitivity of 0.69%, and a frequency deviation rate (FDR) of 0.014 GHz. These results indicate that the sensor offers reliable and precise permittivity detection, particularly for vegetable s materials. Therefore, the proposed microwave sensor is well-suited for food-related applications, such as evaluating the quality and freshness of perishable vegetable goods.

Keywords Microwave sensor · Single-port · Interdigital capacitor · Electromagnetic coupled · Permittivity

Extended author information available on the last page of the article

Published online: 22 December 2025

1 Introduction

Microwave sensors have emerged as a highly promising solution for various sensing applications due to their ability to perform accurate, non-contact, and real-time characterization of materials [1]. These sensors operate by exploiting the interaction between microwave electromagnetic fields and materials under test, where the material's electrical properties such as relative permittivity, permeability, and loss tangent (tan δ) affect the behavior of the transmitted or reflected signal [2]. This principle has led to the development of numerous microwave-based sensors for a wide range of fields, including non-destructive testing [3], biomedical diagnostics [4, 5], material analysis [6], chemical sensing [7], and environmental monitoring [8]. The increasing demand for rapid, cost-effective, and highly sensitive material characterization methods has placed microwave sensors at the forefront of modern sensor research and development.

One of the most significant advantages of microwave sensors is their ability to provide label-free, contactless measurement of material properties [9]. Microwave sensors allow direct interaction with the target material, preserving its physical and chemical integrity [10]. Furthermore, these sensors are capable of penetrating dielectric materials, making them suitable for applications involving layered or embedded structures [11]. Additionally, microwave sensors can be integrated with planar circuits, allowing for compact and cost-effective system designs, which are compatible with modern printed circuit board (PCB) fabrication technologies [12]. Their sensitivity to dielectric changes enables detection of even small variations in material composition, which is crucial for monitoring chemical reactions, detecting biological specimens, or distinguishing between different material types [13].

Recent developments in microwave sensor technology have focused primarily on enhancing sensitivity, expanding the range of detectable permittivity, and improving selectivity toward various types of materials. Resonator-based structures, including T-resonator [14], split-ring resonator (SRR) [15] and complementary split-ring resonators (CSRR) [16, 17] have been proposed to increase the field interaction with test materials and to enable multi-band operation. These advances are particularly useful for applications requiring precise dielectric characterization, especially in the detection of materials with known or limited permittivity ranges.

However, most existing microwave sensor designs predominantly focus on detecting known permittivity materials such as RO-5880, RO-4003, RO-3006, FR-4, and TM-10. While these standard dielectric substrates are useful for calibration and benchmarking, they do not reflect the diversity and complexity of real-world materials. Particularly, these designs fall short in handling vegetable samples whose dielectric properties are less predictable and vary with factors such as water content, aging, and degradation. As a result, they are generally not equipped to determine the permittivity or assess the quality of vegetable samples. Sensors in [18–22], for example, primarily focus on solid materials, and their normalized sensitivity remain relatively low (≤ 0.042), particularly when considering detection of low-permittivity or lossy materials. Vegetable samples such as carrot, cucumber, tomato, and potato are important to observe due to their sensitivity to freshness and spoilage. The ability to detect changes in permittivity for such samples can provide valuable insights into their

internal condition and overall quality [23]. For example, the degradation of vegetable matter due to moisture loss or microbial activity alters its dielectric properties, which in turn affects its microwave response [24]. Therefore, a sensor with the capability to detect vegetable samples is critically needed for determining their permittivity and assessing whether the samples remain suitable for consumption.

To address the limitations found in previous microwave sensor designs, this work proposes a single-port microwave sensor operating at 1.9 GHz, capable of detecting both solid and vegetable samples (which are determined based on polynomial equation) across a broad permittivity range of 1 to 9.8. The proposed design adopts a single port configuration with ELC combined with IDC resonator to achieve excellent sensing performance, high accuracy and sensitivity. It not only supports the detection of conventional dielectric substrates but also extends its capability to characterize vegetable samples, filling a critical gap in current sensor applications. The primary contributions of this work include the design and implementation of a compact microwave sensor based on a single-port architecture, which enables efficient characterization of both solid and vegetable samples. In particular, the simplified structure reduces fabrication complexity while preserving high measurement accuracy over a broad permittivity range. Furthermore, the sensor exhibits strong capability in detecting the dielectric properties of vegetable samples, which is critical for evaluating the quality and freshness of perishable goods. As a result, the proposed sensor offers a practical, versatile, and high-performance solution suitable for advanced material characterization in real-world applications.

2 Working Principle of Microwave Sensor for Permittivity Detection

In this paper, the microwave sensor is proposed for the detection of material permittivity using a resonant frequency shift approach. The overall detection scenario is illustrated in Fig. 1, where the sensor structure, experimental setup, and measurement

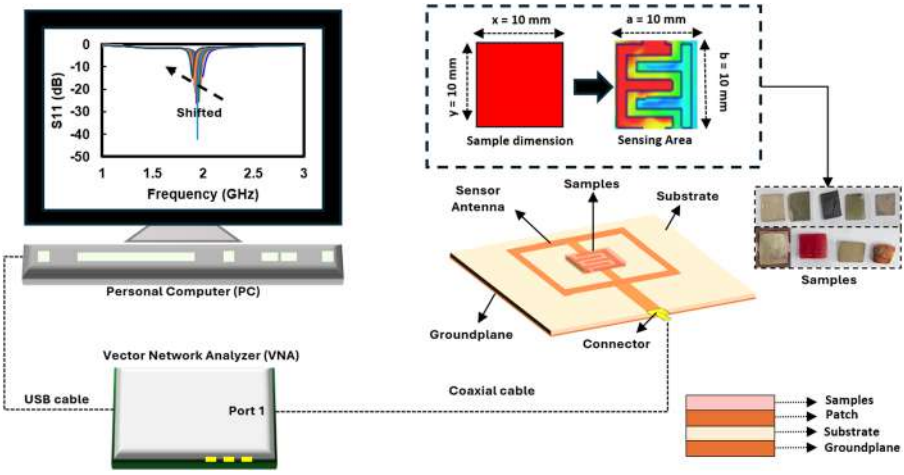

Fig. 1 Proposed scenario for permittivity detection using single port microwave sensor

flow are comprehensively depicted. The sensor is designed to operate at a resonant frequency of 1.9 GHz using an FR-4 substrate, which possesses a relative permittivity (ε_r) of 4.3, a substrate thickness of 1.6 mm, and a dielectric loss tangent of 0.0265. A primary reason for employing microwave frequencies below 2 GHz in the dielectric characterization of vegetable materials is the significantly improved penetration depth achieved in high-moisture, high-loss biological samples. At frequencies above several gigahertz, the strong relaxation behaviour of water and the associated dielectric loss mechanisms result in rapid attenuation of the electromagnetic wave, limiting the effective sensing volume and degrading the signal-to-noise ratio. In contrast, operation below 2 GHz reduces these losses substantially, allowing the field to penetrate deeper into the bulk of the vegetable tissue and enabling a more representative measurement of its internal dielectric properties. This advantage is critical for accurate assessment of moisture content, density variation, and internal structural inhomogeneity, all of which constitute key quality indicators in agricultural and food-engineering applications.

Morevoer, the use of FR4 as a substrate material offers several practical advantages for microwave sensors operating below 2 GHz, primarily due to its low cost, wide availability, and mechanical robustness. At frequencies under 2 GHz, the dielectric losses of FR4 although higher than those of specialized RF substrates remain sufficiently low to maintain an acceptable quality factor and reliable resonant response, making the material suitable for low-to-mid-frequency sensing applications. In addition, FR4's moderate dielectric constant ($\varepsilon r \approx 4.3$) enables compact sensor structures while preserving ease of PCB fabrication using standard industry processes, reducing manufacturing complexity and improving repeatability. These attributes make FR4 particularly advantageous for agricultural and biological material characterization systems, where affordability, durability, and ease of sensor deployment often take precedence over ultra-high-performance requirements.

3 Design and Simulation

3.1 Development Model of Microwave Sensor

The proposed microwave sensor operates based on the principle of perturbation in the electromagnetic field distribution when a material under test (MUT) is introduced in the sensing region. This area is precisely dimensioned to be 10 mm × 10 mm x 1 mm and is optimized to match the physical dimensions of the samples used in the experiment. The MUTs are solid form with identical length and width (a = 10 mm, b = 10 mm), ensuring full coverage of the sensing region and uniform interaction with the sensor.

Moreover, the sensing process involves placing the sample on the patch region of the antenna, which is connected via a coaxial cable to a Vector Network Analyzer (VNA). The VNA is employed to measure the S_{11} parameter, which reflects the input reflection coefficient of the antenna with resonant frequency of 1.9 GHz. The antenna is connected to port 1 of the VNA, and the S_{11} data is transferred in real time to a personal computer (PC) via a USB connection. Furthermore, when a material is placed

on the sensing area, the effective dielectric constant of the region increases depending on the permittivity of the sample. This change results in a shift in the antenna's resonant frequency toward lower frequencies, as illustrated in Fig. 1. The degree of this shift is directly related to the dielectric constant of the sample. Higher permittivity materials cause greater shifts, while lower permittivity materials induce smaller or negligible changes.

The proposed microwave sensor is developed into three different models to optimize its performance for permittivity sensing. Each model features a structural modification aimed at enhancing resonance characteristics and improving electric field (E-field) concentration in the sensing region.

The development of the microwave sensor models is illustrated in Fig. 2a, beginning with model 1, which comprises a microstrip patch antenna with a rectangular sensing area (interdigital capacitor) directly connected to the feedline. To enhance sensitivity, model 2 is derived by rotating the IDC of model 1 by 90° to the right, effectively increasing the current path within the sensing region and improving electric field interaction. Building upon this, Model 3 is developed by rotating only the sensing area of model 2 by 90° to the left, a structural refinement that enhances impedance matching and promotes stronger localization of the electric field within the sensing zone, making model 3 structurally the most optimized configuration.

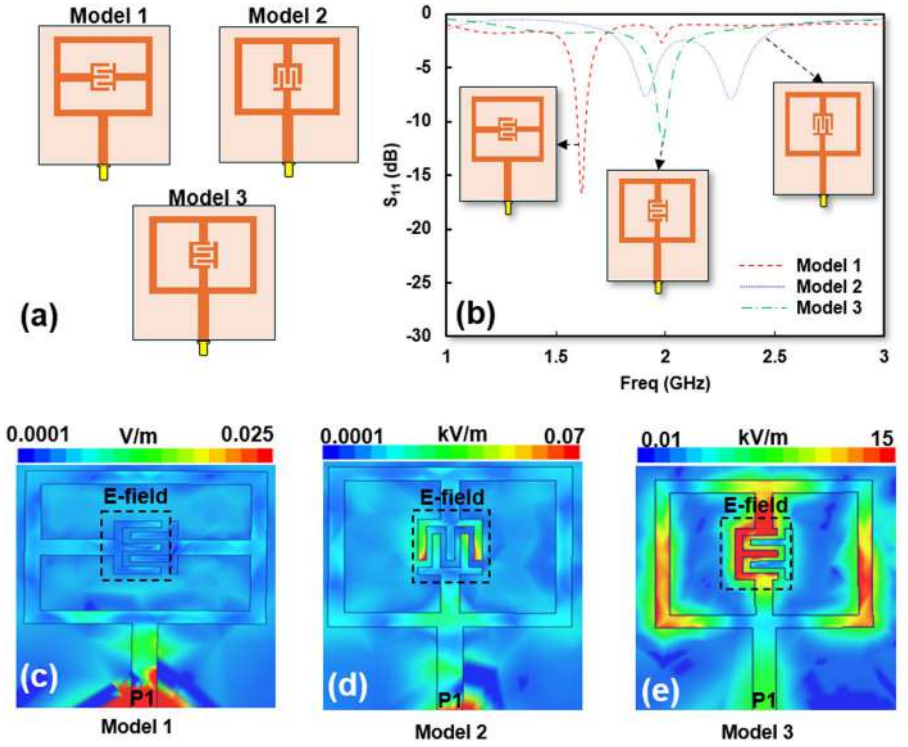

Fig. 2 Development models and simulation result of proposed single port microwave sensor; (**a**) Development models, (**b**) Simulation of S_{11}, (**c**) E-field for model 1, (**d**) E-field for model 2, (**e**) E-field for model 3

The simulated return loss (S_{11}) results shown in Fig. 2b provide insight into the resonance behavior of each model. Model 1 resonates at 1.62 GHz with a return loss of − 16.58 dB, indicating strong impedance matching and effective coupling, initially suggesting it as the most optimal design. In comparison, model 2 exhibits dual resonances at 1.91 GHz and 2.3 GHz but with higher return loss values of − 7.65 dB and − 7.92 dB respectively, suggesting weaker matching and less stable resonance. Model 3 resonates at 1.9 GHz with a return loss of − 11.8 dB, slightly inferior to model 1 in terms of coupling strength. Based solely on return loss, model 1 appears superior. However, further analysis through electric field distribution reveals a deeper perspective on their sensing capabilities.

Figure 2c displays the electric field (E-field) distribution for model 1, where the field intensity is relatively weak and poorly confined within the IDC region, ranging only from 0.0001 V/m to 0.025 V/m. This low E-field magnitude limits interaction with the material under test, indicating insufficient electric coupling for effective permittivity sensing. To overcome this limitation, model 2 incorporates a rotated IDC structure as shown in Fig. 2d, which results in improved E-field intensity reaching up to 0.07 kV/m and better concentration along the IDC region, enhancing sensitivity. Nevertheless, the field distribution remains somewhat dispersed and lacks uniformity which can impact sensing precision.

A more significant improvement is observed in model 3 illustrated in Fig. 2e, which exhibits the highest electric field concentration among the three designs. With E-field intensity peaking at 15 kV/m, the field is highly localized within the central sensing area, ensuring robust interaction with the sample material. This strong field confinement greatly enhances permittivity detection accuracy and reliability, especially for identifying subtle dielectric variations. Thus, while model 1 shows the best return loss, model 3 ultimately emerges as the most effective configuration overall when both electromagnetic and sensing performance are considered, combining improved coupling, structural refinement, and high electric field localization essential for advanced sensing applications.

Moreover, to show relation between resonance frequency, capacitance and the permittivity of proposed sensor, the equivalent circuit based on R, L and C component has been proposed in the revised paper as shown in Fig. 3.

Figure 3a illustrates that the proposed sensor can be represented using lumped R–L–C elements. The equivalent circuit is implemented in AWR MWO 2009, where the microstrip line at the input port (characteristic impedance $Z_0 = 50$ is modeled by $L_1 = 1.642\text{nH}$ and $C_1 = 0.00841\ \text{nF}$. The inductive branches of the ELC structure are characterized by $L_2 = 4.4\ \text{nH}$, $L_3 = 1.52\ \text{nH}$, $L_4 = 0.000218\ \text{nH}$, $L_5 = 0.000781\ \text{nH}$, $L_6 = 0.000244\ \text{nH}$, $L_7 = 20.26\ \text{nH}$, $L_8 = 0.246\ \text{nH}$, and $L_9 = 0.00542\ \text{nH}$. To avoid a short circuit between the resonator and the ground plane, a coupling capacitance $C_g = 0.001\text{nF}$ is incorporated into the model.

The interdigital capacitor section of the sensor is modeled by $R_r = 153\ \text{O}$, $C_r = 0.00106\text{nF}$, and $L_r = 1.66\ \text{nH}$, along with the inductive elements $L_{10} = 4.597\ \text{nH}$and $L_{11} = 1.84\ \text{nH}$. In this analysis, the dielectric under test is treated as a capacitive load $C_s$connected in parallel with the intrinsic sensor capacitance C_r. Variations in the sample's permittivity modify the value of C_s,

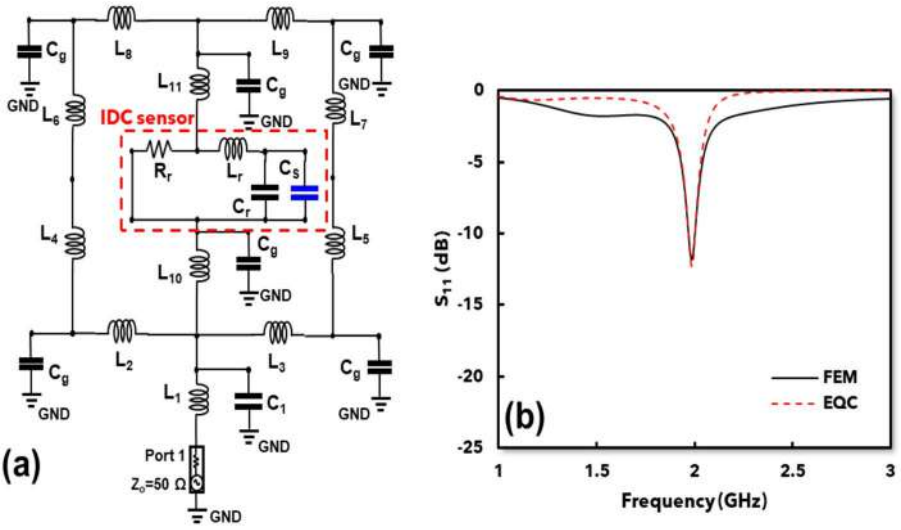

Fig. 3 Simulation circuit model of proposed sensor; (**a**) equivalent circuit of proposed sensor, (**b**) comparison between Finite Element Modelling (FEM) and Equivalent Circuit (EQC)

thereby changing the total capacitance of the resonator and consequently shifting its resonance frequency. Hence, the resonant frequency of the proposed structure can be evaluated using the following expression:

$$f_r = \frac{1}{2\pi\sqrt{L\ (C_r + \ C_S)}} \tag{1}$$

Furthermore, Fig. 3b demonstrates that the Finite Element Method (FEM) simulation results exhibit excellent agreement with those obtained from the equivalent circuit model, with both predicting a resonant frequency of $f_r = 1.9$ GHz. This consistency confirms that the proposed equivalent circuit accurately replicates the behaviour observed in the FEM-based analysis.

3.2 Determination Location of Sensing Area from Proposed Microwave Sensor

Figure 4 illustrates the simulation results and the structural layout of the proposed microwave sensor. As depicted in Fig. 4a, the reflection coefficient S_{11} of the antenna remains below −10 dB within the operational bandwidth, indicating good impedance matching and minimal signal reflection at the resonant frequency. The structural configuration of the microwave sensor is shown in Fig. 4b, while the overall dimensions of the antenna and its structural parameters such as lengths, widths, and gap spacings are annotated in the figure and further detailed in Table 1. The dimension of the sensor antenna is defined by its resonant frequency and the properties of the substrate material. The patch antenna's width (W) and length (L) are calculated using the following equation:

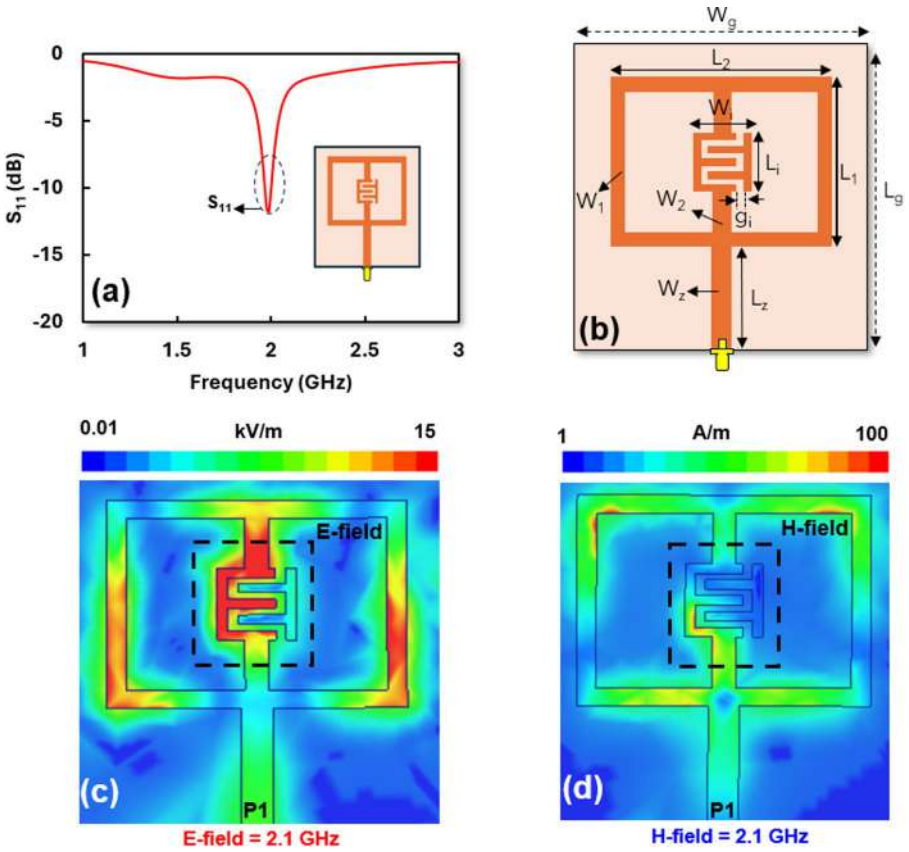

Fig. 4 Simulation result and design of proposed microwave sensor; (**a**) Simulation of S_{11}, (**b**) structure of proposed single port microwave sensor, (**c**) E-field concentration at f_r = 1.9 GHz, (**d**) H-field concentration at f_r = 1.9 GHz

Table 1 Dimension of proposed microwave sensor

Parameters	Dimension (mm)
W_g	50
L_g	50
W	38
L	29
W_r	10
L_r	10
W_1	2.5
W_2	1.3
W_3	3
W_p	4
L_p	17

$$W = \frac{c}{2f\sqrt{\frac{\varepsilon_r + 1}{2}}} \tag{2}$$

$$\varepsilon_{reff} = \frac{\varepsilon_r + 1}{2} + \frac{\varepsilon_r - 1}{2}\left(1 + 12\,\frac{h}{W}\right)^{-1/2} \tag{3}$$

$$\Delta L = 0.412 \times h \times \frac{(\varepsilon_{reff} + 0.3)\left(\frac{w}{h} + 0.264\right)}{(\varepsilon_{reff} - 0.258)\left(\frac{w}{h} + 0.8\right)} \tag{4}$$

$$L_{eff} = \frac{c}{2f_o\sqrt{\varepsilon_{reff}}} \tag{5}$$

$$L = L_{eff} - 2\,\Delta L \tag{6}$$

W and L represent the width and length of the patch respectively (mm); f_o refers to the resonant frequency (GHz); ε_r is the dielectric permittivity of the substrate; ε_{reff} denotes the effective permittivity of the substrate at the given resonant frequency; h represents the thickness of the substrate (mm); and ΔL accounts for the edge effects caused by fringing fields around the patch (mm).

The electric field (E-field) distribution at the resonant frequency f_r = 1.9 GHz as shown in Fig. 3c is concentrated at both the edges and central region of the IDC structure, indicating peak intensity areas during operation, with field magnitude reaching up to 15 kV/m (red regions denote maximum intensity).

Complementing this, Fig. 4d shows the distribution of the magnetic field (H-field) at the same resonant frequency. The H-field is observed to be primarily concentrated within the microstrip channel gap, particularly around the feedline and the meandered sections of the patch. Although the H-field distribution follows the current flow path, its maximum intensity, represented in amperes per meter (A/m), is lower compared to the peak E-field intensity. This contrast indicates that the microwave sensor exhibits predominantly capacitive behaviour due to the stronger electric field component. Therefore, the structure of the proposed microwave sensor is more suitable for use as a microwave sensor rather than as an antenna

3.3 Simulation of Microwave Sensor for Detection of Permittivity, tan delta and Thickness of SUT

Furthermore, Fig. 4 presents a comprehensive simulation analysis of the proposed microwave sensor designed for microwave sensing applications, particularly targeting permittivity detection within the range of 1 to 10. Utilizing the High Frequency Structure Simulator (HFSS), simulations were conducted to evaluate the sensor's frequency response and its correlation with the varying dielectric properties of materials under test. As shown in Fig 5a, the return loss (S_{11}) characteristics of the sensor demonstrate a distinct resonance frequency shift as the relative permittivity (εr) increases, with the resonance frequency decreasing from 1.984 GHz at εr = 1 to 1.904 GHz at εr = 10. This monotonic and predictable shift highlights the sensor's high sensitiv-

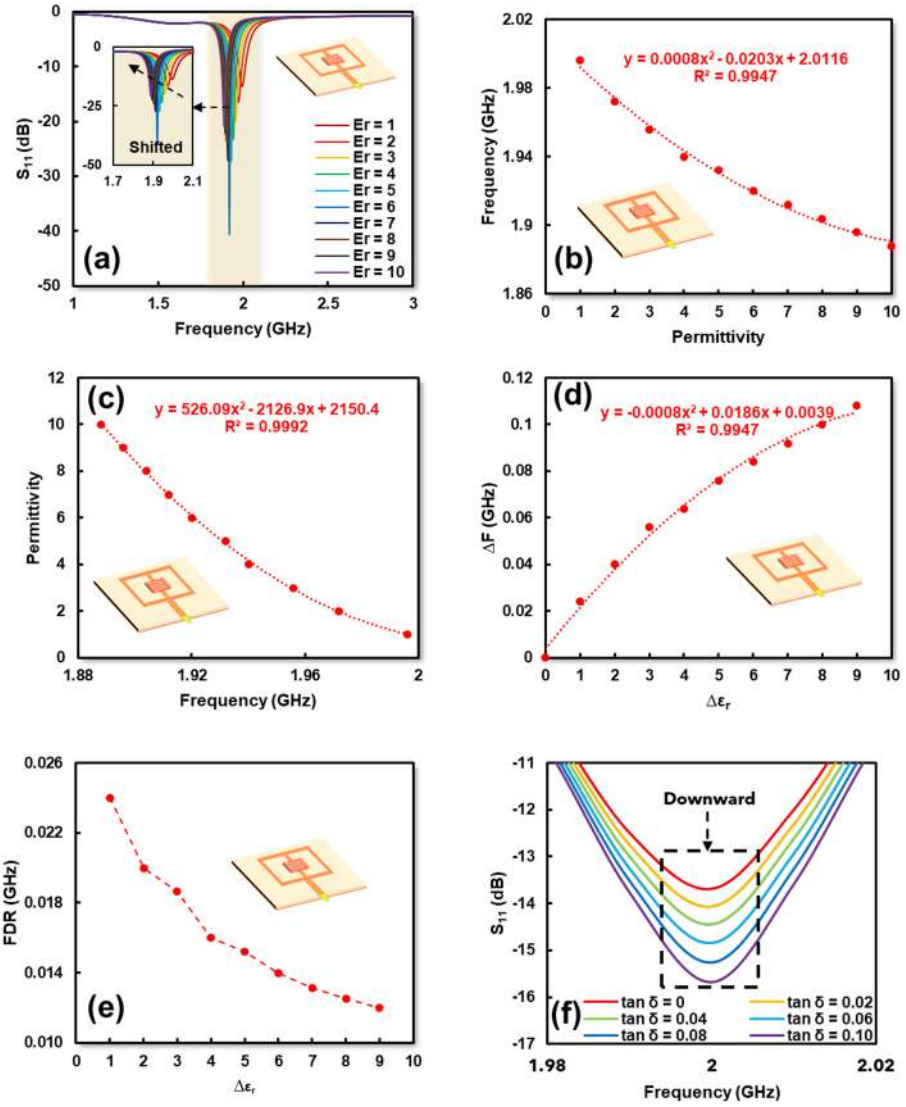

Fig. 5 Simulation using proposed single port microwave sensor; (**a**) Correlation between frequency and permittivity, (**b**) Fitting curve for frequency detection, (**c**) Fitting curve for permittivity detection, (**d**) ΔF of proposed microwave sensor, (**e**) FDR of proposed microwave sensor, (**f**) Simulation detection of tan delta with range of 0–0.1

ity to the dielectric environment in its sensing region, confirming its suitability for microwave sensing especially in distinguishing materials based on their permittivity.

To further quantify this behavior, Fig. 5b introduces a polynomial fitting curve that models the relationship between resonance frequency and relative permittivity by equation:

$$f_r = 0.0008\,(\varepsilon_r)^2 - 0.0203\,(\varepsilon_r) + 2.0116 \quad (7)$$

Where f_r is resonant frequency (GHz), and ε_r is relative permittivity. This equation exhibits a strong correlation ($R^2 = 0.9947$) which validates the reliability of the sensor for accurate, frequency-based dielectric measurements. Complementing this, Fig. 5c provides an inverse polynomial model aimed at direct sensing applications, enabling the estimation of unknown material permittivity from measured resonance frequencies.

$$\varepsilon_r = 526.09\,(f_r)^2 - 2126.9\,(f_r) + 2150.4 \quad (8)$$

This is the inverse of Eq. (7), allowing the estimation of unknown material permittivity from measured resonant frequency values. The higher accuracy with an R^2 value of 0.9992, reinforcing the robustness of the model across the tested permittivity range. Moreover, Fig. 5d continues this analysis by illustrating the absolute frequency shift (Δf) in response to permittivity changes ($\Delta\varepsilon r$), revealing a nonlinear but consistent trend described by the polynomial:

$$\Delta f = -0.0008\,(\Delta\varepsilon_r)^2 + 0.0186\,(\Delta\varepsilon_r) + 0.0039 \quad (9)$$

Δf stands for frequency shift (GHz), and $\Delta\varepsilon r$ is the change in relative permittivity. The R^2 value of 0.9947 affirms the sensor's dependable frequency responsiveness. Moreover, Fig. 5e evaluates the frequency detection resolution (FDR), indicating that the sensor becomes increasingly sensitive at lower permittivity values, a highly desirable trait for applications requiring fine detection of materials with low εr.

Further analysis depicted in Fig. 5f examines the effect of the dielectric loss tangent (tan δ) on the sensor's performance, a key factor in distinguishing between resistive and capacitive loading. While resistive components cause energy dissipation, capacitive components primarily store energy without substantial losses, and this difference significantly affects the reflection characteristics of the sensor. The downward trend in the S_{11} curves as tan δ increases reflects greater microwave energy absorption by lossy materials, resulting in a reduced reflection magnitude. This trend confirms the sensor's sensitivity to dielectric loss variations, making it particularly applicable for detecting lossy substances such as biological tissues or food products. Table 2 supplements this analysis by presenting quantitative S_{11} values at resonance for each corresponding tan δ, thereby reinforcing the sensor's practical utility in diverse permittivity and loss measurement scenarios.

Table 2 S_{11} values from the simulation results of dielectric Tan δ SUT iterations

Tan δ	S_{11} (dB)
0	−13.68
0.02	−14.06
0.04	−14.44
0.06	−14.84
0.08	−15.25
0.1	−15.67

For a lossless material (tan δ = 0), the S_{11} is recorded at −13.68 dB. As the tan δ increases incrementally to 0.02, 0.04, 0.06, 0.08, and finally to 0.1, the S_{11} decreases progressively to −14.06 dB, −14.44 dB, −14.84 dB, −15.25 dB, and −15.67 dB, respectively. This systematic change in the S_{11} value suggests that the sensor exhibits a high degree of sensitivity to dielectric loss, which can be leveraged to distinguish materials with similar permittivity but different loss tangents.

Moreover, Fig. 6 illustrates the simulated S_{11} response of the proposed microwave resonator when loaded with samples of identical permittivity but varying thicknesses (h = 1.0 mm, 1.2 mm, 1.4 mm, 1.6 mm, and 1.8 mm). The results show that as the sample thickness increases, the resonant frequency exhibits a slight downward shift. This behavior occurs because a thicker dielectric sample increases the effective permittivity in the sensing region, which in turn increases the effective electrical length of the resonator, thereby lowering the resonant frequency. Although the frequency shift is not large, the trend is consistent: thicker samples induce slightly stronger perturbations and hence deeper resonance responses. In addition, the magnitude of S_{11} at resonance becomes marginally more pronounced (more negative) with increasing thickness. This is expected because a thicker sample enhances the electromagnetic coupling between the resonator and the material under test, producing a stronger interaction and deeper reflection coefficient minima. Despite these variations, the overall shape of the S_{11} curves remains stable, demonstrating that the sensor maintains predictable behaviour for the range of thicknesses examined. These results confirm that while thickness variation does influence both the resonant frequency and the resonance depth, the effect is gradual and manageable. Therefore, using a fixed sample thickness such as the 1.58 mm adopted in this work ensures measurement consistency and minimizes additional uncertainty in the extraction of dielectric permittivity.

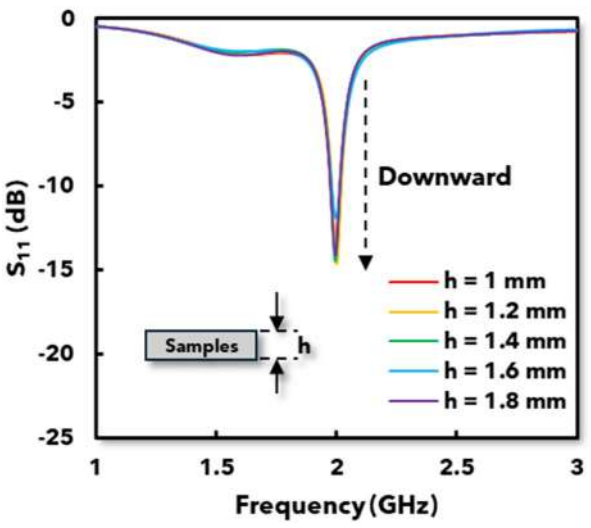

Fig. 6 Simulation results of proposed sensor using different sample thickness with h = 1–1.8 mm

4 Validation and Measurement

4.1 Measurement Process of Proposed Single Port Microwave Sensor

Figure 6 illustrates the experimental validation of the proposed microwave sensor's capability for permittivity detection. Figures 6 and 7a shows the physical setup employed to perform permittivity detection using the fabricated microwave sensor. The sensor is connected to a vector network analyzer (VNA) through port 1 to measure the reflection coefficient S_{11}. The antenna is mounted on a standard PCB substrate, and various test materials are placed over the sensing region. These materials include both dielectric materials such as RO-5880, RO-4003, RO-3006, FR-4, and TM-10, as well as vegetable samples including cucumber, tomato, potato, and carrot. The measurement was conducted at an ambient temperature of 25 °C, within a frequency range of 1 to 3 GHz. A frequency sweep step of 0.004 GHz was used. All samples had identical dimensions of 10 × 10 mm and identical thickness.

To evaluate the accuracy of the fabricated sensor, a comparison between the simulated and measured S11 responses for a reference dielectric material is presented in Fig. 7b. Both results display a similar resonant behaviour, confirming the

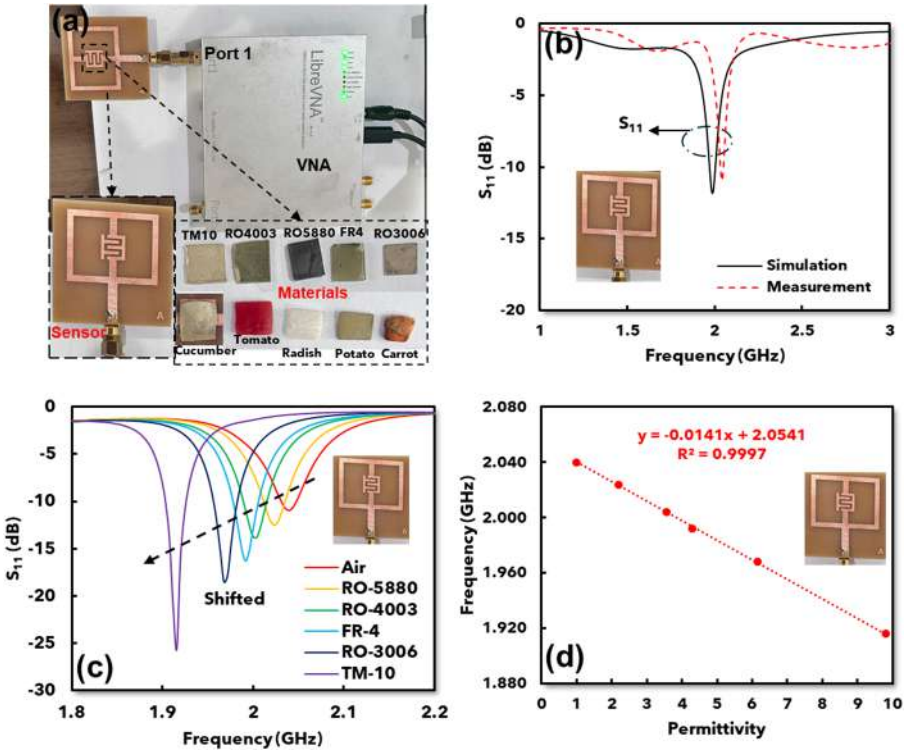

Fig. 7 Measurement of proposed single port microwave sensor for known permittivity materials; (**a**) Setup for detection using microwave sensor, (**b**) Simulation and measurement result, (**c**) Response of frequency with permittivity changes, (**d**) Fitting curve for permittivity detection

sensor's accuracy. In simulation, the resonant frequency is 1.98 GHz with an S_{11} value of −11.814 dB, while the measured result shows a slightly higher frequency of 2.04 GHz and an S_{11} of −10.96 dB. Therefore, to assess the performance of the fabricated sensor and identify any deviations from the simulated behaviour, an error analysis is performed by comparing the resonance frequencies obtained from both simulation and measurement.

$$\text{Error} = \frac{(\text{Measured frequency} - \text{Simulated frequency})}{\text{Simulated frequency}} \times 100\% \quad (10)$$

The error result indicates a frequency deviation of approximately 3.03%, which is relatively small and within acceptable limits for practical sensor implementations. Slight discrepancy between the measured and simulated results can be attributed to several factors. First, fabrication tolerances inherently introduce minor dimensional inaccuracies during the production process. Variations in substrate thickness, conductor width, or misalignment during photolithography can alter the sensor's effective electrical length, thus shifting the resonance frequency. Second, material property variability, particularly the dielectric constant (εr) of the FR4 substrate used also contributes significantly to this deviation. Although simulations often use a nominal permittivity value (typically $\varepsilon r \approx 4.4$), in reality, the permittivity of FR4 can vary from 4.3 to 4.6. These small changes in εr can have a measurable impact on the resonant behavior of the sensor. Moreover, connector losses, soldering effects, and differences in boundary conditions between simulation and experimental setups may also influence the results. The close match of 3.03% between the two curves validates the sensor's performance and confirms its effectiveness in practical permittivity sensing applications.

Building on this validation, Fig.7c demonstrates the sensor's response to six different dielectric materials with known permittivity values. The plot shows the measured S_{11} responses for six different known dielectric materials, with their specifications provided in Table 3.

As evident from the plotted curves, increasing permittivity values cause a systematic shift in the resonant frequency toward lower frequencies. This trend is consistent with the simulation results and highlights the sensor's strong dielectric sensitivity. Among the materials tested, Air exhibits the highest resonant frequency due to the absence of dielectric loading, while TM-10, possessing the highest relative permittivity, results in the lowest resonant frequency. The downward shift in resonant fre-

Table 3 Specifications of materials under test

Materials	Thickness	Tan δ	Relative Permittivity
Air	1.58 mm	0	1
Rogers RT/duroid 5880 (tm)	1.58 mm	0.0009	2.2
Rogers RO4003 (tm)	1.58 mm	0.0027	3.55
FR4_epoxy	1.58 mm	0.0265	4.3
Rogers RO3006 (tm)	1.58 mm	0.0025	6.15
Rogers TMM 10i (tm)	1.58 mm	0.002	9.8

quency as permittivity increases further supports the sensor's potential for precise dielectric property estimation.

To quantify this relationship, Fig. 7d displays a polynomial fitting curve that quantifies the relationship between permittivity and resonant frequency based on the measured data. The inverse relationship is characterized by a linear trendline with a high coefficient of determination $R^2 = 0.9997$, indicating excellent linearity given by the equation:

$$f_r = -0.0141(\varepsilon_r) + 2.0541 \tag{11}$$

εr denotes the material's relative permittivity, while *fr* represents the resonant frequency (GHz). The high accuracy of this fitting model confirms the sensor's reliability and robustness for practical use. In conclusion, the results in Fig. 7 validate the simulation-based analyses and confirm the practical viability of the microwave sensor for permittivity detection. The experimental data not only align with simulation trends but also prove the sensor's accuracy in measuring both engineered and natural dielectric materials. The strong linear correlation between frequency shift and permittivity simplifies the detection process and provides a reliable basis for material characterization.

4.2 Validation and Performance of Microwave Sensor for Permittivity Detection

To validate the accuracy of the proposed sensor in detecting materials with known permittivity, a series of measurements were conducted using reference dielectric samples. The results demonstrated high consistency between the measured and reference permittivity values, thereby confirming the sensor's reliability and precision. The accuracy of the sensor when using materials with known permittivity can be seen in Table 4.

The minimum error was observed with RO-4003 at only 0.02%, yielding a nearly perfect accuracy of 99.98%. Accuracy values for all samples are above 97%, with most exceeding 99%, confirming the sensor's effectiveness in detecting subtle changes in dielectric properties.

To further assess the sensor's precision and its responsiveness to dielectric variations, key performance metrics were calculated based on the frequency response of the microwave sensor to known permittivity materials. These metrics include the absolute frequency shift (Δf), normalized sensitivity (NS), and frequency detection resolution (FDR), which collectively evaluate the sensor's sensitivity, accuracy, and

Table 4 Comparison measurements from single Port microwave sensor for known permittivity materials

Samples	Permittivity	Error (%)	Accuracy (%)
Air	1	0.05	99.95
RO-5880	2.2	3.03	96.97
RO-4003	3.55	0.02	99.98
FR-4	4.3	2.35	97.65
RO-3006	6.15	0.79	99.21
TM-10	9.8	0.14	99.86

capability to detect minor changes in permittivity. The following equations describe how these parameters are derived and provide deeper insight into the sensor's operational effectiveness [25].

$$\Delta \mathrm{f} \; = \; (f_{unloaded} - \; f_{loaded}) \tag{12}$$

The notation Δf represents the frequency shift (GHz), which is the difference between the unloaded resonant frequency and the loaded resonant frequency. This parameter quantifies the absolute change in frequency due to the introduction of a dielectric sample.

$$\mathrm{NS} \; = \frac{1}{\Delta \varepsilon_r} \; \times \left(\frac{f_{unloaded} - \; f_{loaded}}{f_{unloaded}} \right) \; \% \tag{13}$$

Defines Normalized Sensitivity (%), which provides a dimensionless measure of the frequency shift relative to the change in relative permittivity $\Delta\varepsilon_r$ and normalized against the unloaded frequency. This value is useful for comparing sensor sensitivity across different materials or designs, regardless of absolute values.

$$\mathrm{FDR} \; = \frac{\Delta \mathrm{f}}{\Delta \varepsilon_r} \tag{14}$$

Describes the Frequency Detection Resolution (FDR), which expresses how much the resonant frequency (GHz) changes per unit change in relative permittivity. A higher FDR value indicates the sensor's enhanced capability to distinguish subtle variations in permittivity, making it especially effective for applications requiring high-resolution dielectric measurements.

Based on this validation, the sensor was subsequently employed to evaluate the permittivity of various vegetable samples. A polynomial fitting equation in Fig. 6b, derived from the measured data of known permittivity samples, was used as the basis for this estimation. By applying the established equation, the dielectric properties of vegetable samples such as carrot, cucumber, tomato, and potato were successfully determined. This approach ensures that the permittivity values of the vegetable samples are estimated with high accuracy, leveraging the correlation developed from well-characterized reference materials.

Figure 8 illustrates the permittivity detection performance of the proposed microwave sensor when applied to vegetable food materials. Figure 8a shows the relationship between the frequency shift and the change in permittivity for various vegetable food samples. The linear fitting given by the equation:

$$\Delta \mathrm{F} = 0.0141(\Delta \varepsilon_r) \; - \; 4\mathrm{E} \text{ - } 05 \tag{15}$$

ΔF represents frequency shift (GHz), while $\Delta\varepsilon_r$ stands for change in relative permittivity. With a high coefficient of determination $R^2 = 0.9997$ demonstrates that the sensor provides a predictable and stable response even when tested on biological materials with varying water content and internal structure. This result supports the

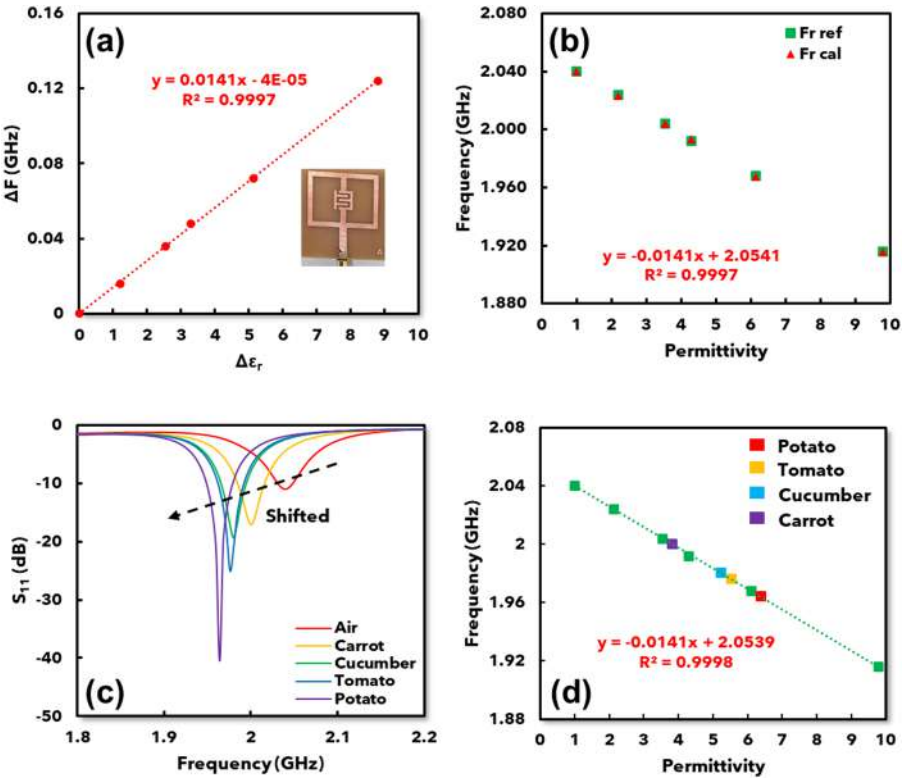

Fig. 8 Measurement of proposed single port microwave sensor for vegetable samples; (**a**) ΔF of proposed microwave sensor, (**b**) Comparison permittivity from calculation and reference, (**c**) Response of frequency with permittivity changes, (**d**) Correlation between frequency and permittivity of vegetable samples

earlier simulation and measurement findings and confirms that the sensor maintains consistent performance across diverse material types.

To further confirm the accuracy of the proposed sensor, a direct comparison between predicted and reference permittivity values is presented in Fig. 8b. This comparison uses the polynomial fitting Eq. (11) and shows an excellent match between the two data sets. The close alignment, supported by an R^2 of 0.9997, indicates that the sensor can reliably estimate the dielectric constant of vegetable samples using a simple frequency-based approach.

The effectiveness of the sensor in distinguishing between different vegetable samples is shown in Fig. 8c, which displays the measured S_{11} responses for several samples, including Air, carrot, cucumber, tomato, and potato. Each sample produces a unique resonance dip, and as the permittivity increases, a clear downward shift in resonant frequency is observed. Air produces the highest frequency response while potato shows the lowest, reflecting its higher moisture content. This consistent shift across samples highlights the sensor's sensitivity and its capability to resolve small variations in dielectric properties. These results are also consistent with earlier dielec-

tric measurements and confirm the sensor's reliability in detecting complex biological materials. The corresponding data for frequency shifts is summarized in Table 5.

Finally, to validate the mathematical model used in predicting permittivity from frequency readings, Fig. 7d presents the fitted curve relating resonant frequency to permittivity for the vegetable samples. The strong linear trend, based on the same Eq. (10): $f_r = -0.0141(\varepsilon_r) + 2.0541$ and an R^2 of 0.9997, confirms that the sensor's response is uniform across both engineered and vegetable samples. This further supports its practicality for real-time dielectric measurements with minimal recalibration or complex processing.

5 Comparison with Previous Work

In order to show the novelty of these works, Table 6 presents a comprehensive comparison of the proposed microwave sensor with existing designs in literature. Operating at 1.9 GHz, the proposed IDC-ELC microwave sensor supports a wide permittivity detection range from 1 to 9.8 and is capable for detecting both solid and vegetable samples using a single port configuration. This offers a distinct advantage over other reported sensors, which are generally limited to solid material detection.

For instance, the previous sensor [20], which employs a U-slot antenna structure, operates at 2.53 GHz and detects permittivity within a narrower range of 1 to 4.13. It is restricted to solid samples and achieves a frequency detection resolution (FDR) of 0.012 and an accuracy of 96%, yet its normalized sensitivity (NS) is relatively low at 0.0015. Similarly, the T-shaped and dual T-shaped resonator-based sensors reported in [19, 22] operate at multiple frequencies—1.64/2.43 GHz and 1.81/2.34 GHz respectively to covering permittivity ranges up to 6.15. These sensors also utilize single port configurations and attain high accuracy levels of up to 99.31%. However, their NS values vary significantly while previous work [22] shows NS values of 0.009/0.006 and [19] reports 1.15/0.16, indicating variability in sensitivity performance. These sensors are also limited to solid sample detection. In contrast, dual-port designs such as the dual split-ring resonator (SRR) in previous work [18] and the nested CSRR [21] exhibit broader FDR values of 0.29 and 0.47, respectively, but lower accuracy levels of 85% and 87%. Their higher NS values of 0.039 and 0.042 suggest reduced precision in permittivity estimation, and like others, they cannot detect vegetable samples.

Overall, the sensitivity performance presented in Table 6 demonstrates that the proposed IDC–ELC microwave sensor exhibits competitive sensing performance relative to existing resonator- and antenna-based approaches. Most prior designs show

Table 5 Frequency shifts of vegetable samples

Samples	Frequency (GHz)	S_{11} (dB)	Calculated Permittivity
Air	2.04	−10.96	1.00
Carrot	2.00	−17.05	3.83
Cucumber	1.98	−19.4	5.25
Tomato	1.976	−25.13	5.53
Potato	1.964	−40.4	6.38

Table 6 Comparison of the proposed microwave sensor with existing works

References	Method	f_r (GHz)	Permittivity Range	Samples	Port Configuration	Sensing Performance			Capability for Vegetable Samples
						FDR	Acc. (%)	NS	
[20]	Antenna with U-Slot	2.53	1–4.13	Solid	Single	0.012	96	0.0015	No
[22]	T-Shaped Resonator	1.64/2.43	1–6.15	Solid	Single	0.16/0.16	95.99/95.16	0.009/0.006	No
[19]	Dual T-Shaped Resonator	1.81/2.34	1–6.15	Solid	Single	0.12/0.002	99.3/99.31	1.15/0.16	No
[18]	Dual SRR	2.27	1–4.3	Solid	Dual	0.29	85	0.039	No
[21]	Nested CSRR	3.37	1–4.3	Solid	Dual	0.47	87	0.042	No
This work	IDC-ELC Microwave sensor	1.9	1–9.8	Solid Vegetable	Single	0.014	98.94	0.69	Yes

frequency deviation ratios (FDR) ranging from 0.012 to 0.47, with nested CSRR and dual-SRR structures achieving high sensitivities at the expense of increased complexity and dual-port configurations. In comparison, the proposed sensor achieves an FDR of 0.014 using simple single-port architecture, indicating that a comparable level of permittivity resolution can be obtained even with a compact, low-frequency (<2 GHz) structure. Moreover, while previous works report narrow permittivity ranges (typically 1–4.3 or 1–6.15), the proposed design maintains high accuracy (98.94%) across a significantly broader permittivity span (1–9.8), confirming its robustness for heterogeneous materials. The normalized sensitivity (NS) value of 0.69 further distinguishes the sensor from prior works, whose NS values remain below 0.05, demonstrating substantially enhanced responsiveness to dielectric variations. Importantly, unlike earlier studies that are limited to solid engineering substrates, the proposed sensor uniquely supports real vegetable samples, validating their applicability for high-loss, moisture-rich materials while preserving high sensitivity and measurement stability.

The proposed microwave sensor demonstrates a well-balanced performance, achieving an FDR of 0.014 and a high accuracy of 98.94%, along with a moderate NS value of 0.69 indicating a reasonable trade-off between sensitivity and measurement stability. Most notably, it is the only sensor in this comparison capable of accurately sensing both solid and vegetable samples. This capability is enabled by the implementation of a polynomial fitting equation derived from known permittivity samples, allowing for precise estimation of unknown vegetable food materials. This highlights the versatility and robustness of the proposed design for practical microwave sensing applications.

However, the present study is limited to the characterization of small, freshly cut vegetable samples, which were selected to ensure consistent placement, stable contact with the interdigital capacitor (IDC) sensing region, and high repeatability during the measurement process. While this approach is appropriate for validating the sensor's fundamental performance, it does not fully represent real-world conditions in which whole vegetables with irregular shapes and varying surface curvatures must be assessed. Additionally, the current setup does not incorporate a dedicated fixture to maintain uniform coupling when evaluating larger or uncut samples, which may influence measurement accuracy. Future work will therefore focus on extending the proposed sensor to accommodate whole-vegetable characterization, including the development of mechanical fixtures to stabilize samples of varying geometries. Further studies will also involve systematic investigations of freshness degradation over time to evaluate the sensor's capability for real-time quality assessment in practical agricultural and supply-chain environments.

6 Conclusion

The proposed microwave sensor, which integrates an Electric Field Coupled (ELC) resonator with an Interdigital Capacitor (IDC) structure has proven to be an effective and accurate tool for permittivity detection of both solid and vegetable food materials. Operating at a resonant frequency of 1.9 GHz and designed with a single-port

configuration maintaining an S_{11} value below −10 dB, the sensor ensures stable and efficient signal reflection characteristics. Utilizing perturbation theory, the sensor accurately detects permittivity changes by monitoring shifts in the resonant frequency when materials are introduced into the high electric field region of the resonator. A polynomial fitting model, developed from reference measurements on materials with known permittivity ranging from 1.0 to 9.8, enables precise estimation of unknown dielectric properties. The sensor achieved a high accuracy rate of 98.94%, a normalized sensitivity of 0.69%, and a frequency detection resolution (FDR) of 0.014 GHz, reflecting its high responsiveness and precision in detecting even small changes in permittivity. These performance metrics affirm the sensor's suitability for applications that demand reliable dielectric characterization, particularly in food technology, where it can be effectively used to assess the quality, composition, and freshness of perishable vegetable products.

Supplementary Information The online version contains supplementary material available at https://doi.org/10.1007/s11220-025-00708-0.

Author Contributions F.KS., S.A and M.N.K wote the main manuscript, R. D.M, L.S, D.A.C and T.F prepare the figure plan, I.S, Z.Z and N.A.S supervised the main manuscript.

Data Availability No datasets were generated or analysed during the current study.

Declarations

Competing Interests The authors declare no competing interests.

References

1. Nikkhah, N., et al. (2024). Highly sensitive differential microwave sensor using enhanced spiral resonators for precision permittivity measurement. *IEEE Sensors Journal, 24*(9), 14177–14188. https://doi.org/10.1109/JSEN.2024.3374282
2. Liu, C., et al. (2024). Microwave sensors and their applications in permittivity measurement. *Sensors*. https://doi.org/10.3390/s24237696
3. Ghattas, A., et al. (2025). Detecting defects in materials using nondestructive microwave testing techniques: A comprehensive review. *Applied Sciences*. https://doi.org/10.3390/app15063274
4. Juan, C. G., et al. (2021). Microwave planar resonant solutions for glucose concentration sensing: A systematic review. *Applied Sciences*. https://doi.org/10.3390/app11157018
5. Kamili, J. B., & Bandi, K. K. (2024). Glucose concentration evaluation in blood samples using novel microwave microwave sensor. *Microsystem Technologies*. https://doi.org/10.1007/s00542-024-05716-w
6. Haq, T. (2020). Extremely sensitive microwave sensor for evaluation of dielectric characteristics of low-permittivity materials. *Sensors (Switzerland)*. https://doi.org/10.3390/s2007191
7. Abdulkarim, Y. I., et al. (2020). The detection of chemical materials with a metamaterial-based sensor incorporating oval wing resonators. *Electronics*. https://doi.org/10.3390/electronics9050825
8. Limpiti, T., et al. (2025). Implementing a low-cost non-destructive microwave sensor to monitor the real-time moisture content of rubber wood in industrial dehydration processes. *Sensors*. https://doi.org/10.3390/s25103053
9. Ali, L., et al. (2021). Design and optimization of microwave sensor for the non-contact measurement of pure dielectric materials. *Electronics*. https://doi.org/10.3390/electronics10243057

10. Dhingra, N., & Saluja, N. (2025). Application of radio frequency microwave sensors to identify adulteration in mustard oil. *Food Analytical Methods*. https://doi.org/10.1007/s12161-025-02766-2
11. Oliveira, J. G. D., & Junior, J. G. D. (2020). A new planar microwave sensor for building materials complex permittivity characterization. *Sensors (Switzerland)*. https://doi.org/10.3390/s20216328
12. Alahnomi, R. A., et al. (2021). Review of recent microwave planar resonator-based sensors. *Sensor Review, 2267*(21), 1–38.
13. Mansour, R., et al. (2020). Development of a resonant microwave sensor for sediment density characterization. *Sensors*. https://doi.org/10.3390/s20041058
14. Alahnomi, R. A., et al. (2020). Accurate characterizations of material using microwave t-resonator for solid sensing applications. *Telkomnika (Telecommunication Computing Electronics and Control), 18*(1), 99–105. https://doi.org/10.12928/TELKOMNIKA.v18i1.14880
15. Ye, W., et al. (2022). An improved split-ring resonator-based sensor for microfluidic applications. *Sensors*. https://doi.org/10.3390/s22218534
16. Harnsoongnoen, S., & Buranrat, B. (2023). Advances in a microwave sensor-type interdigital capacitor with a hexagonal complementary split-ring resonator for glucose level measurement. *Chemosensors*. https://doi.org/10.3390/chemosensors11040257
17. Oliveira, J. G. D., Pinto, E. N. M. G., et al. (2020). Csrr-based microwave sensor for dielectric materials characterization applied to soil water content determination. *Sensors*. https://doi.org/10.3390/s20010255
18. Al-Gburi, A. J. A. (2022). Solid characterization utilizing planar microwave resonator sensor. *Applied Computational Electromagnetics Society Journal, 37*(2), 222–228. https://doi.org/10.13052/2022.ACES.J.370211
19. Alam, S. (2023). Integrated microwave sensor and microwave sensor based on dual T-shaped resonator structures for contact and noncontact characterization of solid material. *IEEE Sensors Journal, 23*(12), 13010–13018. https://doi.org/10.1109/JSEN.2023.3273008
20. Alam, S. (2025). Close quarters permittivity detection based on tagging microwave sensor for solid material characterization close quarters permittivity detection based on tagging microwave sensor for solid material characterization. *Progress in Electromagnetics Research C, 154*, 21–29. https://doi.org/10.2528/PIERC25010701
21. Rahman, N. A., et al. (2020). High quality factor using nested complementary split ring resonator for dielectric properties of solids sample. *Applied Computational Electromagnetics Society Journal, 35*(10), 1222–1227. https://doi.org/10.47037/2020.ACES.J.351016
22. Alam, S., et al. (2024). Collaboratively far-field and near-field regions for dual-modalities microwave permittivity sensor using T-shaped resonator embedded with IDC. *IEEE Sensors Letters, 8*(7), 1–4. https://doi.org/10.1109/LSENS.2024.3415362
23. Dhingra, N., & Saluja, N. (2024). RF sensor-based adulterant discriminant estimation in mustard oil. *Sensing and Imaging*. https://doi.org/10.1007/s11220-024-00508-y
24. Solyom, K. (2020). Effect of temperature and moisture contents on dielectric properties at 2.45 GHz of fruit and vegetable processing by-products. *RSC Advances, 10*(28), 16783–16790. https://doi.org/10.1039/c9ra10639a
25. Alibakhshikenari, M., et al. (2023). Design of a planar sensor based on split-ring resonators for non-invasive permittivity measurement. *Sensors*. https://doi.org/10.3390/s23115306

Authors and Affiliations

Fitri Kurnia Sari[1] · Syah Alam[1] · Indra Surjati[1] · R. Deiny Mardian[1] · Lydia Sari[1] · Muhammad Nugrah Kusumah[1] · Teguh Firmansyah[2] · Dwi Astuti Cahyasiwi[3] · Zahriladha Zakaria[4] · Noor Azwan Shairi[4]

✉ Syah Alam
syah.alam@trisakti.ac.id

[1] Department of Electrical Engineering, Universitas Trisakti, West Jakarta 11440, Indonesia

[2] Department of Electrical Engineering, Universitas Sultan Ageng Tirtayasa, Banten 42117, Indonesia

[3] Department of Electrical Engineering, Universitas Muhammadiyah Prof. Dr. Hamka, Jakarta 12130, Indonesia

[4] Faculty of Electronic and Computer Engineering and Technology, Universiti Teknikal Malaysia Melaka, 76100 Melaka, Malaysia

Source details

Sensing and Imaging

Formerly known as: Subsurface Sensing Technologies and Applications

Years currently covered by Scopus: from 2006 to 2026

Publisher: Springer Nature

ISSN: 1557-2064 E-ISSN: 1557-2072

Subject area: Physics and Astronomy: Instrumentation | Engineering: Electrical and Electronic Engineering

Source type: Journal

View all documents > | Set document alert | Save to source list

CiteScore 2024
3.3

SJR 2024
0.317

SNIP 2024
0.508

CiteScore | CiteScore rank & trend | Scopus content coverage

CiteScore 2024

$$3.3 = \frac{650 \text{ Citations } 2021 - 2024}{197 \text{ Documents } 2021 - 2024}$$

CiteScoreTracker 2025

$$2.9 = \frac{936 \text{ Citations to date}}{318 \text{ Documents to date}}$$

Calculated on 05 May, 2025

Last updated on 05 January, 2026 • Updated monthly

CiteScore rank 2024

Category	Rank	Percentile
Physics and Astronomy Instrumentation	#75/174	57th
Engineering Electrical and Electronic Engineering	#430/970	55th

View CiteScore methodology > CiteScore FAQ > Add CiteScore to your site

About Scopus

What is Scopus

Content coverage

Scopus blog

Scopus API

Privacy matters

Language

日本語版を表示する

查看简体中文版本

查看繁體中文版本

Просмотр версии на русском языке

Customer Service

Help

Tutorials

Contact us

Back

A Single-Port Microwave Sensor Based on Interdigital Capacitor and Electromagnetic Coupled Structure for Permittivity Detection of Vegetables Materials

Sensing and Imaging • Article • 2026 • DOI: 10.1007/s11220-025-00708-0

Sari, Fitri Kurnia [a] ; Alam, Syah [a] ; Surjati, Indra [a] ; Mardian, R. Deiny [a] ; Sari, Lydia [a] ; +5 authors

[a] Department of Electrical Engineering, Universitas Trisakti, West Jakarta, 11440, Indonesia

Show all information

Abstract

This research proposed a single port microwave sensor designed for permittivity detection of both solid and vegetable samples, utilizing an Electric Field Coupled (ELC) resonator combined with an Interdigital Capacitor (IDC) structure. The sensor operates at a centre frequency of 1.9 GHz and adopts a single-port configuration with a reflection coefficient (S_{11}) maintained below – 10 dB. Permittivity measurement is achieved using perturbation theory, where a shift in the resonant frequency occurs when a material is introduced into the sensing region. This sensing region is defined by the location of maximum electric field concentration within the resonator. A polynomial fitting equation, derived from measurements on known dielectric materials with permittivity values ranging from 1 to 9.8, is used to estimate the permittivity of vegetable samples. The proposed sensor demonstrates high performance, with a measured accuracy of 98.94%, normalized sensitivity of 0.69%, and a frequency deviation rate (FDR) of 0.014 GHz. These results indicate that the sensor offers reliable and precise permittivity detection, particularly for vegetable s materials. Therefore, the proposed microwave sensor is well-suited for food-related applications, such as evaluating the quality and freshness of perishable vegetable goods.

Author keywords

Electromagnetic coupled; Interdigital capacitor; Microwave sensor; Permittivity; Single-port

Indexed keywords

Engineering controlled terms

Dielectric materials; Electric fields; Microwave resonators; Microwave sensors; Natural frequencies; Permittivity measurement; Perturbation techniques; Polynomial approximation; Vegetables

Engineering uncontrolled terms

Coupled resonator; Coupled structures; Electromagnetic coupled; Electromagnetics; Interdigital capacitor; Sensing region; Single-port; Solid samples; Vegetable materials; Vegetable samples

Engineering main heading

Permittivity

Corresponding authors

Corresponding author	S. Alam
Affiliation	Department of Electrical Engineering, Universitas Trisakti, West Jakarta, 11440, Indonesia
Email address	syah.alam@trisakti.ac.id

About Scopus

Scopus blog

Scopus API

Privacy matters

Language

日本語版を表示する

查看简体中文版本

查看繁體中文版本

Просмотр версии на русском языке

Customer Service

Help

Tutorials

Contact us

ELSEVIER

Scopus

This author profile is generated by Scopus

Alam, Syah

Universitas Trisakti, Jakarta, Indonesia • Scopus ID: 57191903622 • 0000-0002-0162-8364

Show all information

346	76	11
Citations by **259** documents	Documents	*h*-index

Set alert | Save to list | Edit profile | More

Beta

Documents (76) | Impact | Cited by (259) | Preprints (1) | Co-authors (125) | Topics (15) | Awarded grants (0)

You can view, sort, and filter all of the documents in search results format.

Export all | Save all to list | Sort by Date (newest)

Article

A Single-Port Microwave Sensor Based on Interdigital Capacitor and Electromagnetic Coupled Structure for Permittivity Detection of Vegetables Materials

0 Citations

Sari, F.K., Alam, S., Surjati, I., ... Zakaria, Z., Shairi, N.A.

Sensing and Imaging, 2026, 27(1), 7

Show abstract Full text Related documents

Article

Independent and asymmetric coupling structure for integrated dual-band bandpass filter with microwave microfluidic milk sensor

0 Citations

Firmansyah, T., Praptodiyono, S., Muttakin, I., ... Iqbal, M., Nugraha

AEU International Journal of Electronics and Communications, 2026, 206, 156186

Show abstract Full text Related documents

Article

Application of LT Code with BCH Precode for Wireless Body Area Network

0 Citations

Sari, L., Alam, S., Mardian, R.D., Surjati, I.

Journal of Electrical and Electronics Engineering, 2025, 18(2), pp. 63–68

Show abstract Full text Related documents

Don't miss out on new publications by this author!

Set document alert

Article

Multifunctional microwave-plasmonic microfluidic sensor utilizing gold nanoparticles embedded in multilayered ring resonator

0 Citations

Firmansyah, T., Alfanz, R., Denny, Y.R., ... Wibisono, G., Kondoh, J.

Sensors and Actuators A Physical, 2025, 385, 116275

Show abstract Full text Related documents

Article • *Open access*

1

SAR Distribution with Different Water Bolus Shapes for Hyperthermia Breast Cancer Treatment

Citations

Hassan, M.M., Lias, K., Buniyamin, N., ... Basri, H.M., Alam, S.

Journal of Advanced Research in Fluid Mechanics and Thermal Sciences, 2025, 128(1), pp. 32–47

Show abstract Full text Related documents

Article • *Open access*

A Broadband Half-Mode Substrate Integrated Waveguide Cavity Antenna with Triple Resonances

2

Citations

Astuti, D.W., Majid, H.A., Alam, S., Setyawan, A.

Progress in Electromagnetics Research C, 2025, 152, pp. 55–66

Show abstract Full text Related documents

Article • Article in Press

Fabric-based Metamaterial-Integrated CPW Antenna for Microwave Tumor Sensing

0

Citations

Razak, I.S.A., Al-Gburi, A.J.A., Said, M.A.M., Alam, S., Zakaria, Z.

IEEE Sensors Journal, 2025

Show abstract Full text Related documents

Article • *Open access*

Broadband HMSIW antenna using a demi hexagonal ring slot for X-band application

3

Citations

Astuti, D.W., Muslim, M., Umaisaroh, U., ... Alam, S., Rahayu, Y.

Sinergi Indonesia, 2025, 29(1), pp. 73–82

Show abstract Full text Related documents

Article

1

A Fabric-Based Double Rectangular Complementary Split Ring Resonator for Wideband Applications

Abd. Razak, I.S., Zakaria, Z., Al-Gburi, A.J.A., ... Alam, S., Palandoken, M.

Progress in Electromagnetics Research C, 2025, 157, pp. 147–158

Show abstract Full text Related documents

Citations

Article

Single-Port Microwave Sensor Using Defected Ground Structure Complementary Split Ring Resonator for Solid Material Characterization

Amer, R.A.B., Shairi, N.A., Said, M.A.M., ... Alam, S., Rahim, S.K.A.

Progress in Electromagnetics Research C, 2025, 158, pp. 139–149

Show abstract Full text Related documents

0

Citations

Previous 1 2 3 4 5 ... 8 Next

Display 10 results

View all references

Document & citation trends

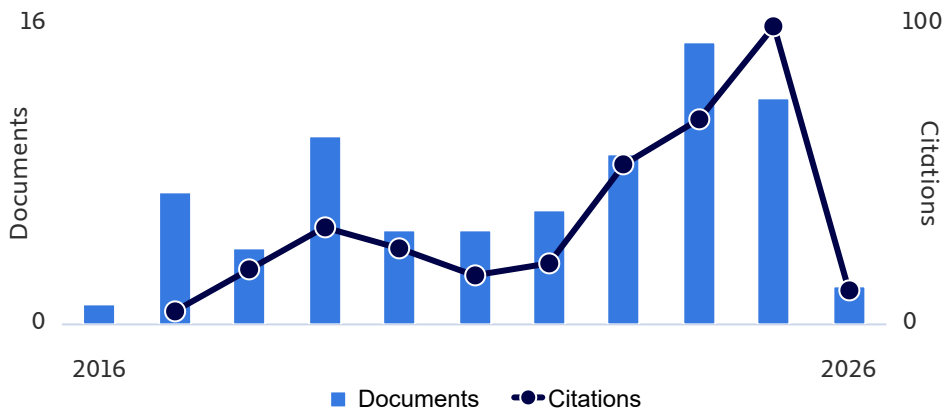

Citation overview Analyze author output

Author Position for 2015 - 2024

First author 49%

29	5	0.69
Documents	Average citations	FWCI

Last author 18%

Co-author 33%

Single author 0%

Show author position details

Back to top

About Scopus

What is Scopus

Content coverage

Scopus blog

Scopus API

Privacy matters

Language

日本語版を表示する

查看简体中文版本

查看繁體中文版本

Просмотр версии на русском языке

Customer Service

Help

Tutorials

Contact us

Return to Search Results

SENSING AND IMAGING

Share This Journal

ISSN / eISSN **1557-2064 / 1557-2072**
Publisher **SPRINGER, ONE NEW YORK PLAZA, SUITE 4600 , NEW YORK, United States, NY, 10004**

General Information

Journal Website	Visit Site	**Publisher Website**	Visit Site
1st Year Published	2000	**Frequency**	Continuous publication
Issues Per Year	1	**Country / Region**	UNITED STATES OF AMERICA
Primary Language	English		

Web of Science Coverage

Collection	Index	Category	Similar Journals
Core Collection	Emerging Sources Citation Index (ESCI)	Instruments & Instrumentation	Find Similar Journals

Search a topic within this journal

Search a topic within this journal... Search

Journal Citation Report™ (JCR)

Journal Citation Reports™ 2025

If this shows your subscription as not active, please log in to https://jcr.clarivate.com directly.

Journal Impact Factor™ (JIF)

2024	2023
Not seeing a JIF? A JCR subscription is required to view the JIF for this journal. If this is an error, please use the "Check Subscription Status" button to contact support.	Not seeing a JIF? A JCR subscription is required to view the JIF for this journal. If this is an error, please use the "Check Subscription Status" button to contact support.
Category: Instruments & Instrumentation	**Category:** Instruments & Instrumentation

Check Subscription Status | Learn About Journal Citation Reports™

Journal Citation Indicator (JCI) NEW METRIC

The Journal Citation Indicator is a measure of the average Category Normalized Citation Impact (CNCI) of citable items (articles & reviews) published by a journal over a recent three year period. It is used to help you evaluate journals based on other metrics besides the Journal Impact Factor (JIF).

2024	2023
0.49	0.51
Category: Instruments & Instrumentation	**Category:** Instruments & Instrumentation

Learn About Journal Citation Indicator

Peer Review Information

Web of Science Reviewer Recognition	No	**Claimed Reviews on Web of Science**	634
Public Reports on Web of Science	No	**Signed Reports on Web of Science**	No
Transparent Peer Review on ScholarOne	No		

Create a free *Web of Science profile* to track your publications, citation metrics, peer reviews, and editing work for this journal.

PubMed® Information

Indexed In	PubMed®	**MeSH® Headings**	Diagnostic Imaging|Radar|Signal Processing, Computer-Assisted|Technology
NLM® ID	101301371		